



XA04C1743

## **Irradiation Induced Tensile Property Change of SA 508 Cl. 3 Reactor Pressure Vessel Steels**

**Se-Hwan Chi\*, Jun-Hwa Hong, Il-Hiun Kuk**

Nuclear Materials Technology Development Team

Korea Atomic Energy Research Institute

### **Abstract**

Irradiation induced tensile property change of four kinds of reactor pressure vessel steels manufactured by different steel refining process was compared based on the differences in the unirradiated and irradiated microstructure. Microvickers hardness, indentation, and miniature tensile specimen tests were conducted for mechanical property measurement and optical microscope (OM) and transmission electron microscope(TEM) were used for microstructural characterization. Specimens were irradiated to a neutron fluence of  $2.7 \times 10^{19} \text{ n/cm}^2$  ( $E \geq 1 \text{ MeV}$ ) at  $288^\circ\text{C}$ . Investigation on the unirradiated microstructures showed largely a same microstructure in that tempered acicular bainite and ferrite with bainitic phase prevailing in the unirradiated condition. Band-shaped segregations were also clearly observed except a kind of materials. A large difference in the unirradiated microstructure appeared in the grain size and carbide microstructure. Of carbide microstructures, noticeable differences were observed in the size and distribution of cementite, and bainitic lath microstructures. No noticeable changes were observed in the optical and thin film TEM microstructures after irradiation. Complicated microstructural state of heat treated bainitic low alloy microstructure prevents easy quantification of microstructural changes due to irradiation. Apparent differences, however, were observed in the results of mechanical testing. Results of tensile testing and hardness measurement show that a steel refined by vacuum carbon deoxidation(VCD) method exhibits the highest radiation hardening behavior. Some of mechanical testing results on irradiated materials were possible to understand based on the initial microstructure, but further investigations using a wide array of sophisticated tools(for example, SANS, APFIM) are required to understand and characterize irradiation induced defects that are responsible for irradiation hardening behavior but are not revealed by conventional TEM.

\* Corresponding author, E-mail: shchi@kaeri.re.kr, Tel:(042)868-2385

*Presented at 1998 IGORR 6, April 29 - May 1, 1998, Taejon, Korea.*

## **I. Introduction**

Analysis and evaluation of tensile properties change have been recognized as one of principle methods in acquiring data necessary for probing the neutron-irradiation sensitivity of reactor structural materials. Incorporation of tensile specimens in the reactor pressure vessel (RPV) surveillance capsules manifest itself the usefulness of the tensile specimens for monitoring the radiation-induced changes in the mechanical properties of RPV steels. Of those data obtainable from tensile tests, measurements on the changes in yield and fracture strength, and total and uniform elongation due to irradiation provide raw data for obtaining first hand informations on radiation hardening and embrittlement, and necessary data for estimating fracture behavior, or for evaluating elastic-plastic fracture toughness through empirical or analytical correlation [1], and also provide strength data necessary for determining fracture toughness value from fracture mechanics specimen testing.

In obtaining these tensile properties from irradiated materials, then, standard, somewhat large size specimens have been used as the specimens used for a RPV surveillance program. In the case of irradiation tests, however, reduction in specimen size has been necessitated by restrictions in the irradiation volume or limitations in the amount of material available from irradiated components, and by the difficulties of handling radioactive materials and by the need of multiplication of specimens [2]. It is worth to note that there have been observed on a number of occasions that the small specimen tensile data scatter is substantially smaller than the large specimen data scatter as long as a sufficient number of grains are maintained in the cross section of the tensile specimen [3].

In this study irradiation induced tensile properties change in four kinds of RPV steels was obtained, and compared the results based on the differences in the unirradiated and irradiated microstructure to explore the irradiation sensitivity of these steels manufactured by different steel refining process.

## **II. Experimental**

### **II.1 Materials and specimen preparation.**

Coupons used for specimen preparation were extracted from four shell forgings which differed in the steel refining process. Chemical composition and steel refining process of the materials are summarized in **Table 1** and the heat treatment conditions of the shell forgings are summarized in **Table 2**. Schematics of each shell forging manufacturing processes are quite similar each other except the major steel refining processes. Coupons, and specimens were machined and prepared from 1/4 T (thickness)

locations of the shell forgings. Fig. 1 shows the configuration of miniaturized tensile specimen used in the present study. Vickers microhardness tests were performed on hardness disc specimens machined from each coupons.

## II.2 Irradiation.

Prepared specimens were irradiated to the neutron fluence of about  $2.7 \times 10^{19}$  n/cm<sup>2</sup> ( $E \geq 1$  MeV) at LVR-15 experimental reactor in the NRI(nuclear research institut) Rez, Czech Republic using a rig CHOUCA MT. Specimens were kept in inert atmosphere(He, Ar) at the pressure of 80 - 140 kPa during irradiation. Six kinds of fluence monitors, i.e., Ti, Cu, Ni, Fe, Nb, and Co, were used at nine locations in the specimen carrier. Irradiation temperature was controlled by six heaters of the rig and twelve thermocouples type K with measuring junction insulated, 1 mm in diameter, six of them being placed just on the heaters middle position, were installed for irradiation temperature measurement. Except the stainless steel nut, all other components of carrier were made of aluminum or aluminum-magnesium alloy(Al-Mg5). Neutron flux and irradiation temperature were about  $2.7 \times 10^{13}$  n/cm<sup>2</sup>. sec and  $288 \pm 10^\circ\text{C}$ , respectively. It is worth to note that the fluence in the present study roughly corresponds to the design end life fluence of a reactor. Fig. 2 shows the schematics of carrier used for irradiation. Details of irradiation are reported elsewhere [4].

## II.3 Microstructural investigation.

For optical microscopy, specimens in size of about 4 x 4 mm were polished to 0.3  $\mu\text{m}$  Al<sub>2</sub>O<sub>3</sub> powder, etched in 1.5~3 % Nital for 10 ~ 20 sec, and examined in Nikon(EPIPHOT-THE) Inverted Microscope. The grain size was determined by the three-circle(or Abrams) procedure of ASTM E-112-88, " Standard Test Methods for Determining Average Grain Size" at x 400. Optical microstructures were also examined at x 400.

Investigation of microstructures and carbide morphology was performed by TEM(JEOL 2000FX). Disc specimens (3 mm  $\Phi$ ) were prepared by a submerged electrolytic jet thinning technique in a solution of 10% perchloric acid and 90% acetic acid at 30 to 35 V of applied voltage. 100 - 200  $\mu\text{m}$  diameter holes were made within about 1 minute on disks polished below 0.1 mm thickness. Perforated specimens were rinsed in clean acetic acid and then in methyl alcohol before TEM observation.

To quantify possible differences in a detailed carbide size and density upon materials on TEM, carbon extraction replicas were prepared. Specimens were extracted from shoulder areas of each tested tensile specimens, and ground and

polished through 0.3 micron alumina. The polished area was moderately etched with 4 % Nital for 60 ~ 120 sec to expose carbide clusters. Specimens were then mounted on a glass slide for carbon coating by vacuum evaporation. A 5 mm length at one end of a 3mm diameter carbon rod was sharpened down to 1 mm dia for evaporation and inserted in a Ladd model 30170 carbon holder. The rod holder was placed in a Veeco high vacuum evaporation chamber. The slide bearing the specimens was placed approximately 13 cm beneath the sharpened carbon rod to avoid specimen heating during evaporation. The carbon rod was evaporated under vacuum. Evaporation of the sharpened rod required approximately 2 minutes at a 20 amp level. A total of three carbon depositions were administered to the specimens to provide a practical carbon layer thickness. The specimen slide was rotated approximately 120° under the evaporation source between each deposition to provide a uniform deposition thickness and prevent inconsistencies due to shadowing and fixture geometry. Carbon specimens were scored into about 2 x 2 mm<sup>2</sup>. Stripping was performed in 10 % HCl + 90 % ethanol solution at about 0.1 ampere for about 4~5 minutes using a platinum wire as a cathode until the scored carbon peeled off. Cu grids of 400 mesh and 3 mm Ø were then used to collect floating replicas. The replicas were then examined by TEM for precipitates morphologies, and were photographed for precipitates size and density determination.

#### **II.4 Mechanical test.**

Tensile tests were performed on an Instron 1122, 1,000 pound capacity, screw-driven load frame. Tests were conducted at ambient temperature at a constant displacement rate of  $8.5 \times 10^{-3}$  mm/sec. A special fixture was fabricated to facilitate loading specimens into grips without deforming the specimen. Load-displacement data were recorded on an X-Y recorder and, in addition, the data were digitized and recorded in a computer-based data bank. An average of 500 load-displacement points per specimen were saved.

Vickers microhardness tests were performed on hardness disc specimens machined from each coupons. An automated Wilson Tukon microhardness tester was used to perform at least 10 indentations per specimens at room temperature. Load and duration were 300 g and 20 sec, respectively. Average DPH values with the standard deviation were automatically obtained from all of the indentation data by using a developed software. Details of the automated hardness tester are reported elsewhere [5].

### III. Results.

#### III.1 Comparison of microstructure.

Photos obtained by optical microscopy(OM) on unirradiated condition of each steels are reproduced in Fig. 3, and those of TEM on unirradiated(thin film and replica) and irradiated specimens(thin film) are seen in Fig. 4(a) and 4(b), respectively. Comparisons of grain size, precipitates and carbide morphology, precipitates number per unit area, and lath microstructure were made based on OM and TEM results in the unirradiated condition, and summarized in Table 3. First of all, from Fig. 3 and 4, it is seen that all materials show largely the same bainitic microstructure in that tempered acicular bainite and ferrite with bainitic phase prevailing in the unirradiated condition irrespective of materials and no noticeable changes were observed in the thin film TEM microstructures after irradiation. This observation on irradiated microstructure of RPV steels already have previously been reported and discussed in detail by Buswell [6]. Band-shaped segregation were clearly observed for A, B, and C except D. As summarized in Table 3, there were some differences in grain size, especially between A and B, C, D. The grain size of A is 50% larger than the B, C and almost double that of D. It is well known that, for austenite grain size control using aluminum nitride particles [7], aluminum and nitrogen levels are controlled to achieve austenite grain sizes in the range ASTM 7 - 10 (10 - 30  $\mu\text{m}$ ) [8]. Accordingly, the absence of aluminum addition in A versus B, C, D can account for the larger grain size.

Round cementites and acicular  $\text{Mo}_2\text{C}$  carbides were found in all steels. No apparent difference was seen in the size of acicular  $\text{Mo}_2\text{C}$  carbides, which were mostly 50 - 100 nm. However, the size of the cementite particle in steel A was about 10 - 20 times larger than that of C and D. Moreover, as seen in Fig. 4(a), large agglomerated islands of round cementites were frequently observed in A, but not in D. The size of the agglomerates in A, mostly larger than 30 $\mu\text{m}$  in length, were larger than the average grain size of A ( $\sim 22\mu\text{m}$ ) as seen in Fig. 4(a). Alloy C showed a larger carbide density than A and D for all three types of carbide morphology. For A and D, with roughly the same number density of carbides, the number of needle-like  $\text{Mo}_2\text{C}$  was a little higher in A than D. Recent results of Minfa Lin et al [9] show that the precipitation of needle-like carbides during tempering is related to the upper-nose temper embrittlement. The long square rod and round carbides in A appear to be precipitated along the lath boundary, but round and needle-like carbides appear to be precipitated along the grain boundary and inside of the lath, respectively.

From Fig. 4(a), it is seen that the lath boundary in A was not developed well

compared to B, C, and D. D showed the narrowest lath width( $2\mu\text{m}$ ) and A showed the widest( $5\mu\text{m}$ ). Interlath carbides were found in A, B, and C as seen in **Fig. 3**, and were thickest in A. A low cooling rate during quenching has been attributed to the growth of interlath carbides [10]. As remarked previously, even the complicated microstructural state of the heat treated bainitic steels prevents easy quantification of possible microstructural changes due to irradiation, it is seen that , at least under the present experimental conditions(OM, TEM) all of the microstructural characteristics in unirradiated condition were unchanged.

### III.2 Tensile and hardness test.

Results of the tensile and Vickers microhardness tests on unirradiated and irradiated specimens are summarized in **Fig. 5** and **6**, respectively. Firstly, it is seen that the tensile strength(yield, ultimate tensile) has increased and ductility(uniform and total) has decreased with the increase in the hardness for all materials after irradiation. The changes in the strength was quite apparent compared to the elongation due to irradiation. Thus, the yield and tensile strength increased for about 5% - 19 %, but the uniform and total elongation decreased only for about 0.5% - 1.4%. In addition, it is seen that the differences in yield strength between materials have enlarged after irradiation. This observation strongly suggests that the degree of radiation sensitivity of each material is different to each other. It is also worth to note that the standard deviations of strength data(yield and tensile) in irradiation condition are quite big compared to those of elongation(uniform and total). This observation can partly be attributed to the possible large differences in the irradiation-induced defects that are responsible to friction hardening after irradiation [11]. The deviation in the irradiated yield strength is the largest among all the tensile parameters measured. Some of these observation may easily be understood through the comparisons of TEM thin film results on irradiated and unirradiated materials. Thus, no appreciable changes in the size, distribution, density, and morphologies of large carbides, which have been reported to have a strong correlation with the fracture related properties of materials, in the irradiation condition strongly imply that there should be no appreciable changes in the tensile properties after irradiation. However, the enlargement of the differences between the yield strength after irradiation between the materials strongly suggests that the degree of radiation sensitivity of each material, including the hardening behavior but not restrict to, is different to each other possibly due to the unidentified irradiation- induced defect microstructures . **Figs. 5(I)** and **5(IV)** show that A exhibits the largest increase in the yield strength and the largest decrease in

the total elongation. Compared to A, D showed moderate increase in the strength but the least decrease in the uniform and total elongation, Fig. 5(III) and 5(IV). This observation can also be assumed to be resulted partly from the differences in the carbide(cementite) size and distribution as compared in Table 3. Thus, compared to A, the narrowest bainitic lath width, the smallest grain and cementite size, well developed lath boundary, well dispersed carbides through the matrix, and free of interlath carbides are assumed to have resulted in this observation. The fracture toughness as well as Charpy impact test data also have shown that D leads other materials [12].

Hardness data in Fig. 6 show that the range of data distribution has increased after irradiation as in the case of yield strength data. It is seen that the increase in A is the largest and vice versa for D. The increase in A (37%) was almost double of D(19%). From the correlation between the yield strength and Vickers microhardness data, no apparent correlation trend was observed mainly due to the scarcity in data.

#### IV. Discussion

As a whole the over-all sensitivity of the materials to neutron irradiation agrees well, within the scatter bound, with the previously reported results on commercial RPV steels except A [13]. However, present result apparently shows that A shows relatively higher sensitivity to irradiation than the other materials: As seen in the Fig. 5(I), the rate of increase in yield strength of A was about 1.8 - 3.4 times higher than those of C and D. It is worth to note that this increase in yield strength at room temperature is chosen as the most sensitive measure of irradiation [14]. Result of Vickers microhardness has also shown that the rate of increase of A to D was about 2. A showed also the largest decrease in total elongation measurements. Comparisons made with the previously reported results [15] also showed that, even for nearly the same fluence, irradiation temperature and chemistry, the yield strength of A appeared to increase about 10 MPa more than the other RPV forging steels. Currently it is hard to explain clearly why only A shows the highest sensitivity to neutron irradiation with nearly the same microstructure when compared with other RPV steels. As noted previously, microstructures revealed by OM and TEM explain well the inferior fracture-related elongation behavior in A as seen in Fig. 5(III) and 5(IV). Most of these observations in elongation may be attributed to the large grain size with the elongated and large, agglomerated carbides often encountered along the grain boundaries in A [16]. However, present results are insufficient and, in some sense, contradict to the highest hardening behavior of A. As seen in Fig. 5(I), A shows nearly the same yield strength with the other steels in the unirradiated condition. Thus, differences between the steels are negligible in the unirradiated condition. This observation is quite reasonable since all the compared RPV steels were

commercially manufactured to the strict requirements of ASME materials code on RPV steel which specifies major factors(variables) affecting the mechanical properties of the RPV steels including the chemistry and heat treatment condition. **Fig. 4(b)** also does not show any modifications after irradiation or any differences between the unirradiated and the irradiated TEM microstructures. With only this observation and results, however, the amplified differences between the yield strength values and the highest hardening behavior of A after irradiation are difficult to explain. Part of these observation may be attributed to the extremely fine size( $< 10$  nm) of irradiation-induced defects which are not easily characterized by conventional TEM [17] and to the different steel refining processes employed [18]. For these irradiation-induced defects as in the case of low copper RPV steels of the present study, irradiation-induced increase in the yield strength, thus, radiation hardening, has recently been remarked by the formation of extremely fine nanovoid-complexes and interstitial loop-complexes as candidates with small phosphides, carbides and nitrides [19]. Further examinations using a wide array of sophisticated tools (for example, SANS, APFIM) are required to understand and fully characterize the extraordinary high radiation hardening behavior of A.

## **V. Conclusions.**

Differences in the irradiation-induced tensile property change for four kinds of commercial RPV steels differing in microstructures partly due to different steel refining processes have been investigated. For nearly the same microstructures before and after irradiation, steel A refined by the vacuum carbon deoxidized process appeared to have the highest sensitivity to neutron irradiation. A showed the highest increase in yield strength and Vickers microhardness, and the largest decrease in total elongation.

Part of these observation can be attributed to and rationalized in terms of microstructural differences characterized by OM and TEM. However, the extraordinary highest hardening behavior in A as envisaged in yield strength measurements after irradiation seems difficult to rationalize based only on the present results partly because of the limited capability of TEM in characterizing the responsible irradiation-induced or enhanced damage microstructures. In this sense, further study using a wide array of advanced, sophisticated tools (for example, SANS, APFIM) are required to understand and fully characterize the irradiation hardening behavior of RPV steels.

## Reference

- [1] W. A. Pavinich, Proceedings of the Second International Symposium on Environmental Degradation of Materials in Nuclear Power Systems-Water Reactors, Monterey, California Sept. 9-12, 1985, pp. 485-495.
- [2] Se-Hwan Chi, Jun-Hwa Hong, and In-Sup Kim, *Scripta Metallurgica et Materialia*, 30 (1994) 1994.
- [3] N. F. Panayotou, R. J. Puigh, and E. K. Opperman, *J. Nucl. Mater.*, 103-104 (1981) 1523.
- [4] Report on the KAERI Sample Irradiation, Nuclear Research Institute Rez plc, DIM-OMV97, Dec. 1997.
- [5] G. R. Odette and G. E. Lucas, Final Report RP-1021-7, 1990, EPRI.
- [6] J. T. Buswell, Examination of materials by electron microscopy. In *Analysis of the Behavior of Advanced Reactor Pressure Vessel Steels Under Neutron Irradiation*. The UK Programme UKAEA, 1983, 281.
- [7] R. H. Sterne and L. E. Steele, *Nucl. Eng. and Design*, 10 (1969)259.
- [8] Marshall Report/LWRSG(PV) 1982. p. 12.
- [9] Minfa Lin, S. S. Hansen, T. D. Nelson, R. B. Focht, ASTM STP 1259, E. G. Nisbett and A. S. Melilli, Eds., ASTM, 1997 (in press).
- [10] S. Ohtani, S. Okaguchi, Y. Fujishiro, and Y. Ohmori, *Metall. Trans. A*, 21A (1990) 877, and Private Communication with Y. R. Lim, Seoul National University.
- [11] D. R. Olander, *Fundamental Aspects of Nuclear Reactor Fuel Elements*, TID-26711-P1, Technical Information Center, Energy Research and Development Administration, 1976. p. 431.
- [12] Unpublished Results, KAERI (1997).
- [13] *Analysis of The Behavior of Advanced Reactor Pressure Vessel Steels Under Neutron Irradiation*, Technical Report Series No. 265, IAEA, Vienna, 1986. pp. 29-35.
- [14] p. 29 in Ref. [13].
- [15] p. 34 in Ref. [13].
- [16] Se-Hwan Chi, G. E. Lucas, J. H. Hong, G. R. Odette, Differences in Mechanical Properties and Microstructure of SA 508 Cl. 3 Reactor Pressure Vessel Steels Manufactured by Different Steel Refining Process, Submitted for publication in *J. Nucl. Mater.*, 1998.
- [17] Recent Progress in Understanding Reactor Pressure Vessel Steel Embrittlement, In *Fundamentals of Radiation Damage and Challenges for Future Nuclear Materials*, Ishino Conference, The University of Tokyo, Collected Abstracts, Dec. 15-16, 1994. pp.30 - 31.
- [18] *Radiation Damage of Structural Materials*, Materials Science Monograph, 79., J.

Koutsky and J. Kocik Eds. Elsevier Pub., 1994. p.70.  
[19] p. 31 in Ref. [17].

Table 1. Chemical composition and steel refining process of SA 508 Cl. 3 steel A, B, C, and D which are differ in steel refining process.

Specimen I. D	SRP*	C	Si	Ni	Mn	Cr	Mo	Cu	P	N	Al
A	VCD	0.18	0.08	0.77	1.40	0.15	0.53	0.06	0.005	0.004	<20ppm
B	VCDA	0.17	0.10	0.82	1.35	0.16	0.50	0.03	0.006	55ppm	0.015
C	SA(I)	0.21	0.24	0.92	1.36	0.21	0.49	0.03	0.007	52 "	0.022
D	SA(II)	0.19	0.20	0.82	1.44	0.15	0.55	0.03	0.006	89 "	0.020

SRP\*: Steel Refining Process, VCD:Vacuum Carbon Deoxidation,

VCDA:Vacuum Carbon Deoxidation plus Aluminum treatment,

SA(I) and SA(II): Silicon deoxidation plus Aluminum treatment in two different factory, I and II.

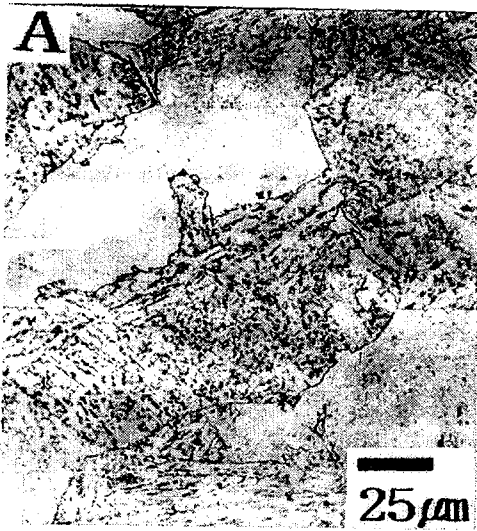
Table 2. Heat treatment condition of material A, B, C, and D.

Material	Heat Treatment Condition
A, B, C	Quenching: 650/690°C (4 hr), 860~900°C (6 hr) Water quenching to 60°C Tempering: 650 ~ 670°C (9~12 hr) Postweld Heat Treatment: 621±14 °C (30 hr)
D	Quenching: 870/897°C (14.2 hr), water quenching Tempering: 650/663°C (12.4 hr), air cooling Postweld Heat Treatment: 595/625°C (14.4 hr), furnace cooling

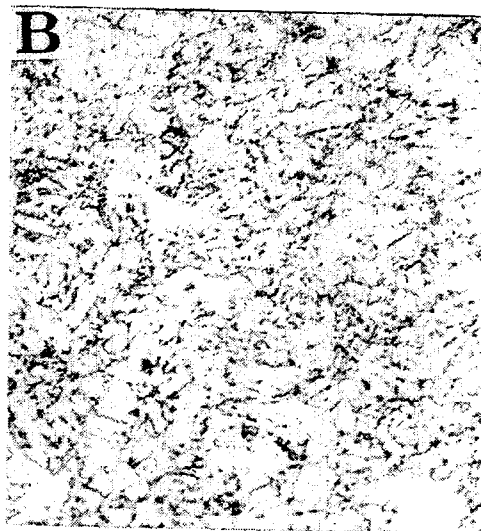
Table 3. Grain size, carbide and precipitates morphology, and bainite lath structure obtained by optical microscope and TEM on thin films and carbon replicas for A, B, C, and D steels.

Material	Grain Size		Precipitates, Carbide, and Bainite Morphology and Lath width( $\mu\text{m}$ )	Remarks
	ASTM	SIZE( $\mu\text{m}$ )		
A	7.6	22	Round(dia: $\sim 0.5 \mu\text{m}$ ), Fine Needle(50~100nm), Agglomerated, large and localized coarse carbides, Underdeveloped lath boundary, lath width: $5 \mu\text{m}$ Coarse interlath carbide. PPTs No: $6 \times 10^7/\text{mm}^2$ Round:Needle=1:0.85	
B	8.7	15	Round(dia:0.05~0.25 $\mu\text{m}$ ), Fine Needle(80 nm), Slightly agglomerated, Semi-underdeveloped lath boundary, lath width: $5 \mu\text{m}$ , Interlath carbide, PPTs No.: $8.5 \times 10^6/\text{mm}^2$ Round:Needle=1: 22	Incomplete replication
C	8.7	15	Round(dia: 0.025 $\mu\text{m}$ , Needle(80nm), Square-like needle(100nm), Three types of carbides morphology, PPTs at GB and matrix, Well developed lath boundary, lath width: $3.5 \mu\text{m}$ , Interlath carbides, PPTs No.: $3.1 \times 10^9/\text{mm}^2$ , Round:Needle:Square Needle=1:1.75:0.46.	
D	9.5	12	Round( $<0.05 \mu\text{m}$ ), Needle(50~100nm), Fine round carbide, Well developed lath boundary, lath width: $2 \mu\text{m}$ , No interlath carbides, PPTs No.: $6.7 \times 10^7/\text{cm}^2$ , Round:Needle=1:0.39.	





(A) VCD



(B) VCDA

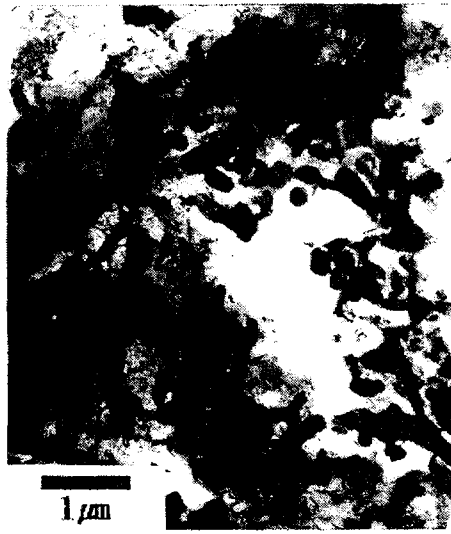


(C) SA(I)



(D) SA(II)

Fig. 3 Optical micrographs of A, B, C, and D steels.



(A) VCD



(B) VCDA



(C) SA(I)



(D) SA(II)

**Fig. 4(a)** TEM(thin film) micrographs of the A, B, C, and D steels.

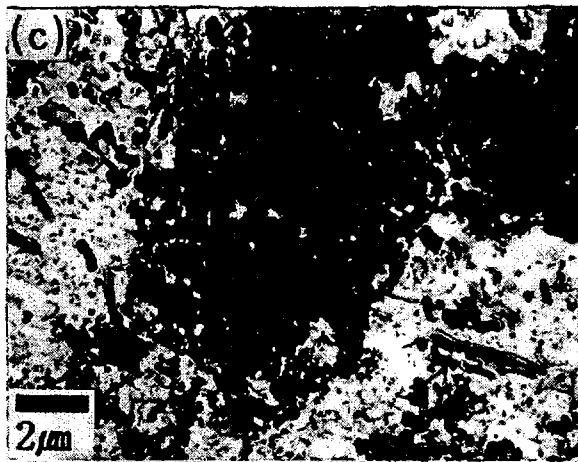
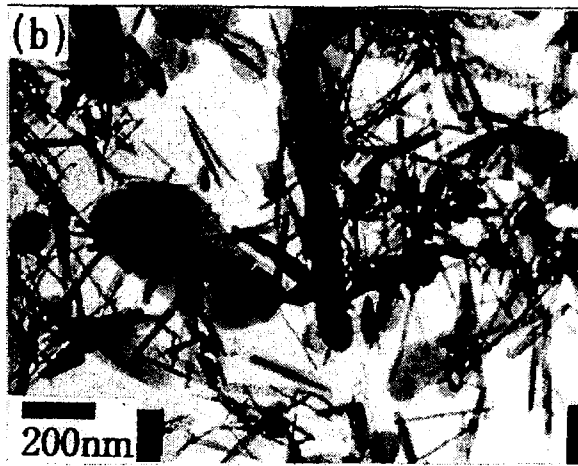
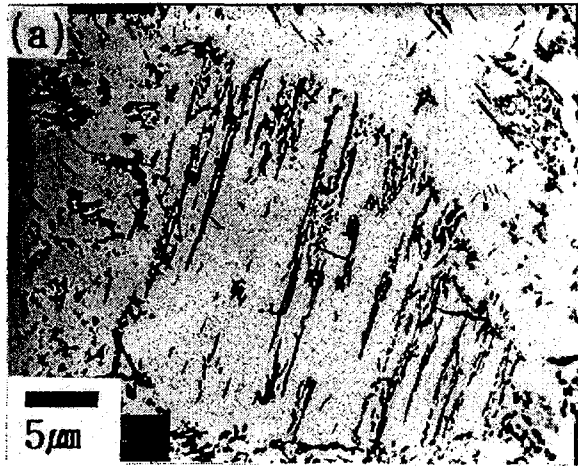


Fig. 4(a).I TEM(carbon replication) micrographs of steel A(VCD).

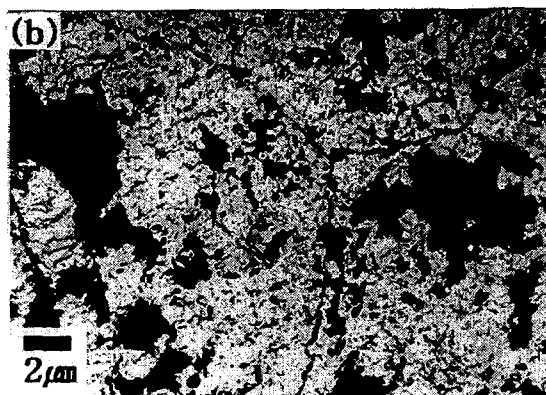
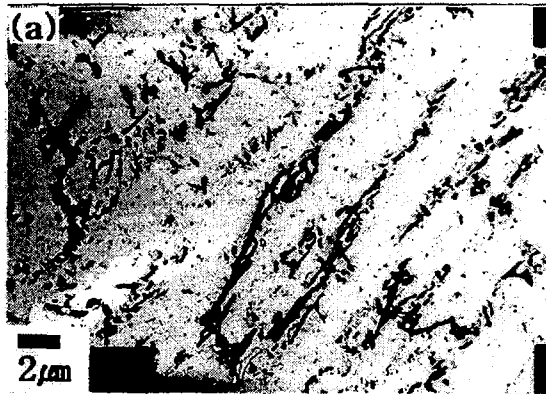


Fig. 4(a).II TEM(carbon replication) micrographs of steel B(VCDA).

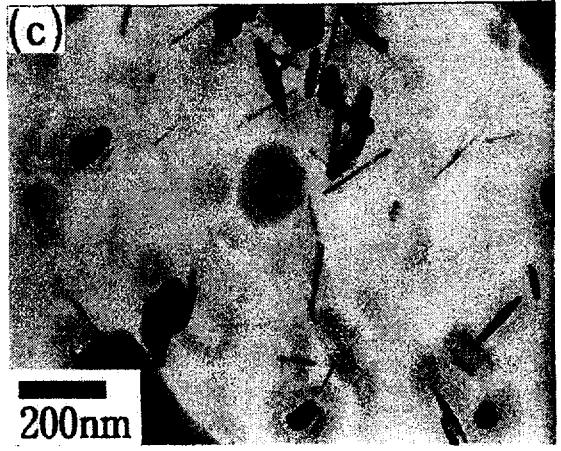
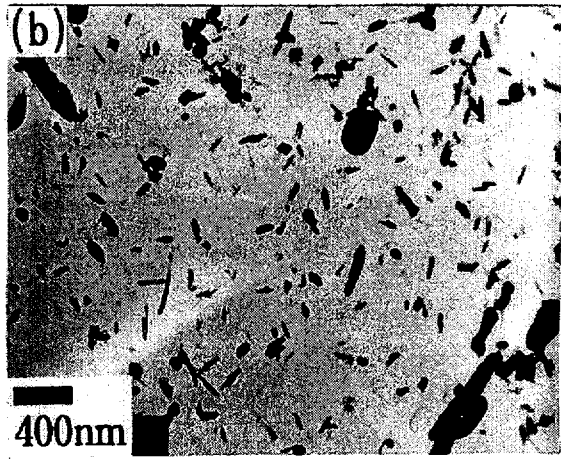
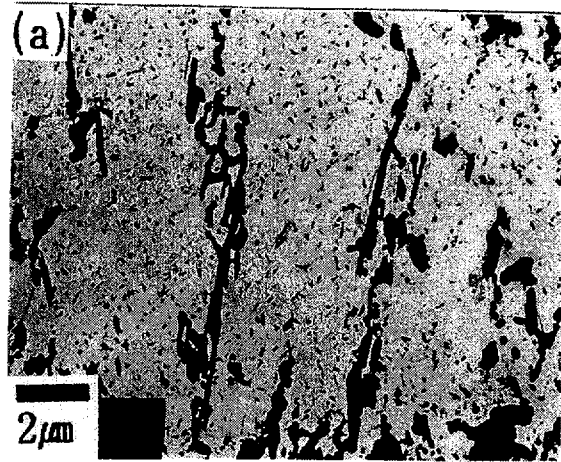
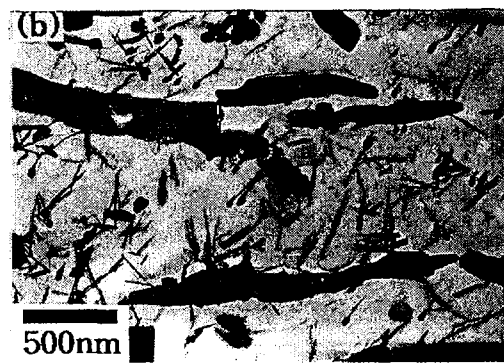
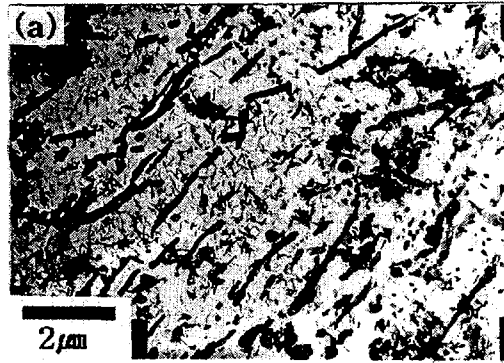


Fig. 4(a).III TEM(carbon replication) micrographs of steel C(SA( I )).



**Fig. 4(a).IV** TEM(carbon replication) micrographs of steel D(SA(II)).

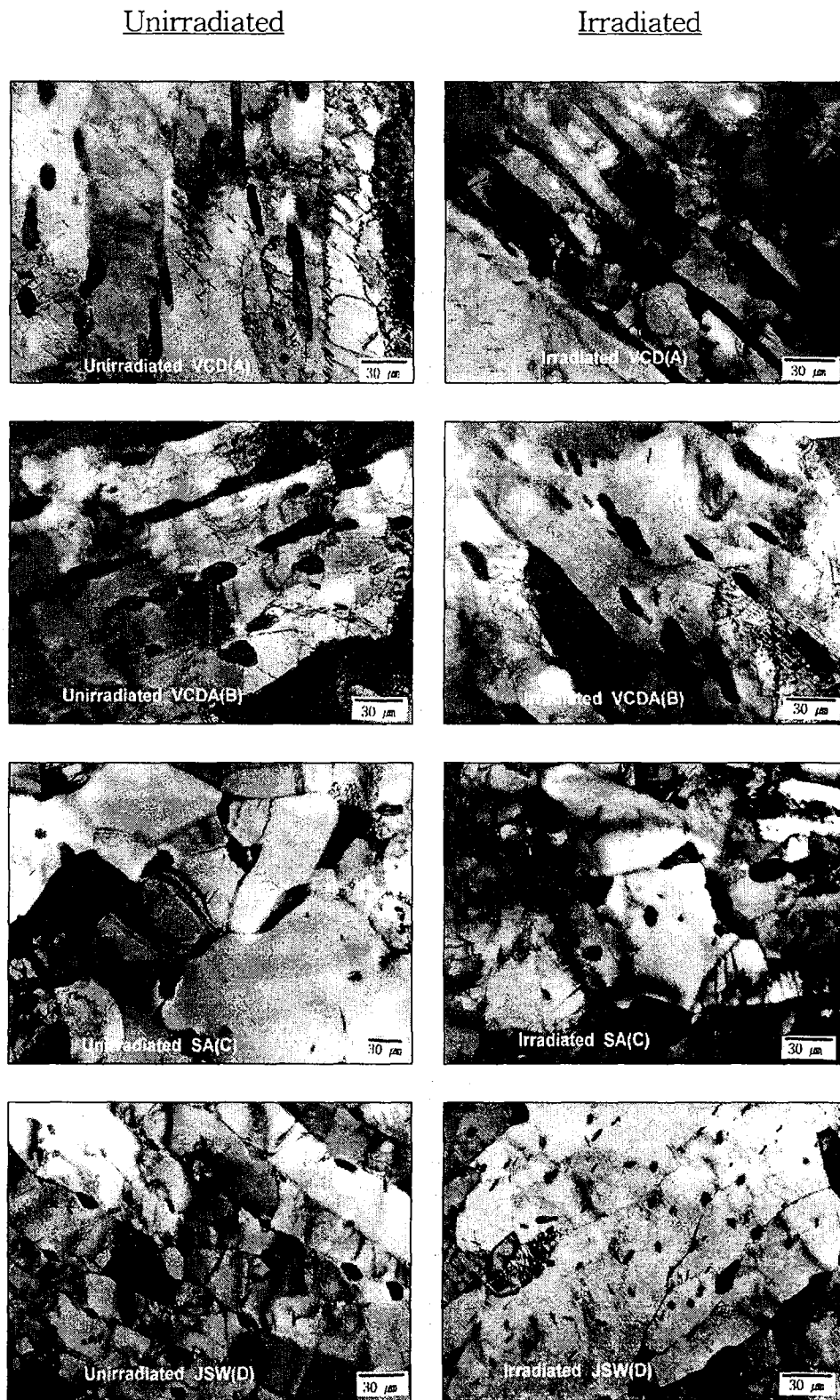


Fig. 4(b) Comparison of TEM microstructure of RPV steels A, B, C, and D before and after irradiation(  $2.7 \times 10^{19}$  n/cm<sup>2</sup>, 288 °C ).

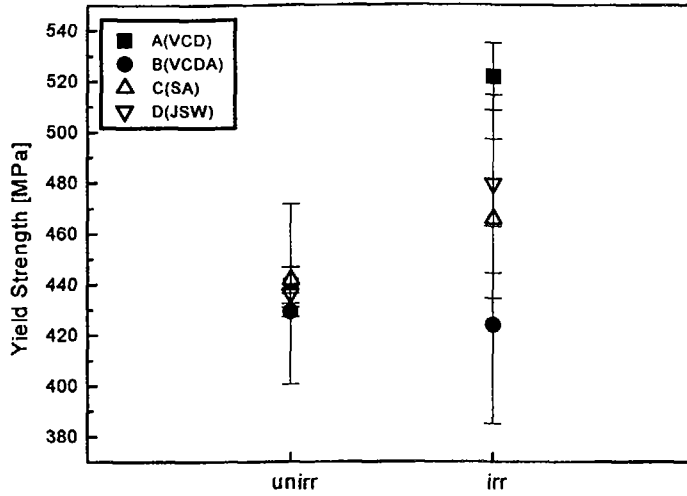


Fig. 5(I) Yield strength change of RPV low alloy steels A, B, C, and D due to irradiation( $2.7 \times 10^{19} \text{ n/cm}^2$ , 288 °C).

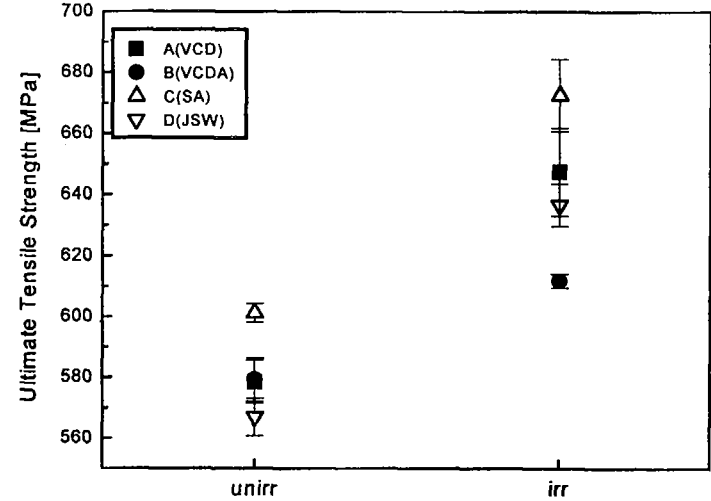


Fig. 5(II) Ultimate tensile strength change of RPV low alloy steels A, B, C, and D due to irradiation( $2.7 \times 10^{19} \text{ n/cm}^2$ , 288 °C).

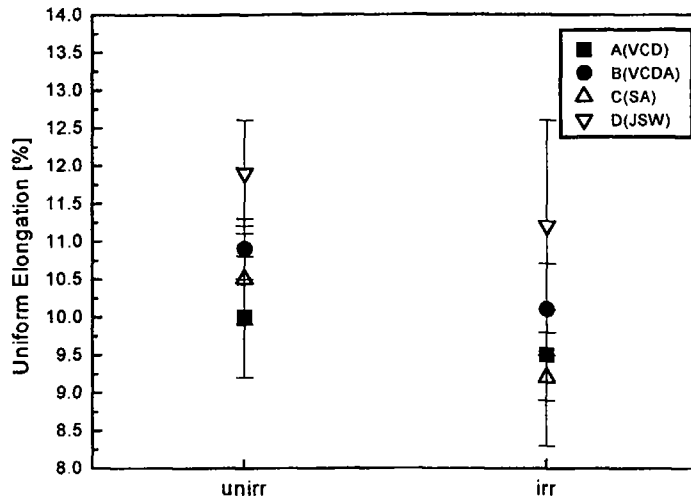


Fig. 5(III) Irradiation induced change of uniform elongation of RPV low alloy steels A, B, C, and D ( $2.7 \times 10^{19} \text{ n/cm}^2$ , 288 °C).

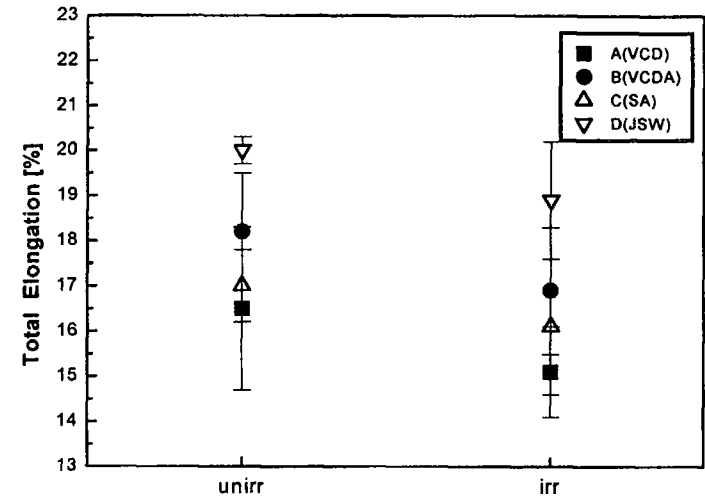
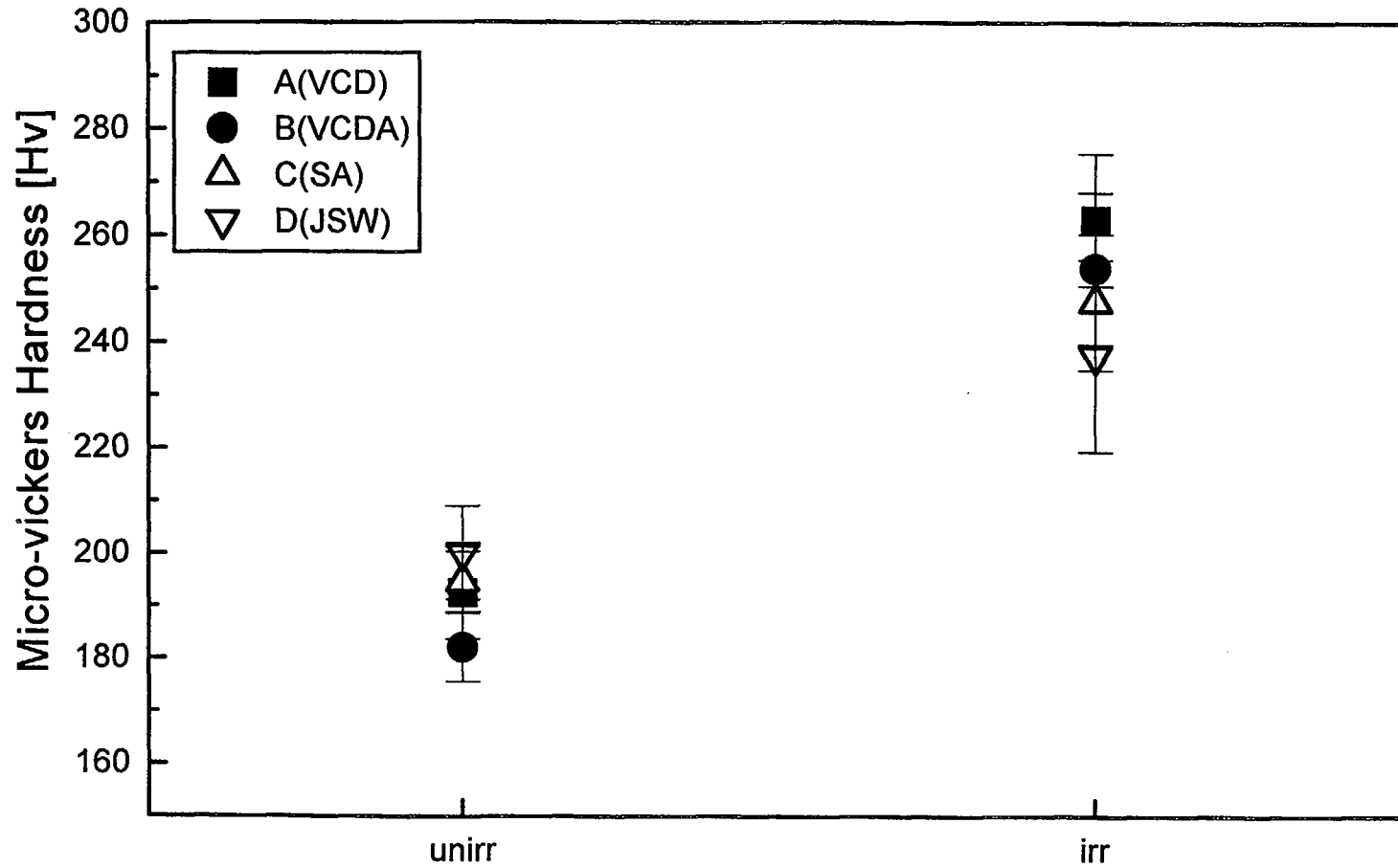


Fig. 5(IV) Irradiation induced change of total elongation of RPV low alloy steels A, B, C, and D ( $2.7 \times 10^{19} \text{ n/cm}^2$ , 288 °C).



**Fig. 6** Irradiation-induced change of Micro-vickers hardness of RPV low alloy steels A, B, C, and D ( $2.7 \times 10^{19} \text{ n/cm}^2$ ,  $288 \text{ }^\circ\text{C}$ ).

